LETTERS
PUBLISHED ONLINE: 3 AUGUST 2015 | DOI: 10.1038/NPHYS3419
nature physics

Long-lived nanosecond spin relaxation and spin coherence of electrons in monolayer MoS_2 and WS_2

Luyi Yang[1], Nikolai A. Sinitsyn[2], Weibing Chen[3], Jiangtan Yuan[3], Jing Zhang[3], Jun Lou[3] and Scott A. Crooker[1]*

The recently discovered monolayer transition metal dichalcogenides (TMDCs) provide a fertile playground to explore new coupled spin–valley physics[1–3]. Although robust spin and valley degrees of freedom are inferred from polarized photoluminescence (PL) experiments[4–8], PL timescales are necessarily constrained by short-lived (3–100 ps) electron–hole recombination[9,10]. Direct probes of spin/valley polarization dynamics of resident carriers in electron (or hole)-doped TMDCs, which may persist long after recombination ceases, are at an early stage[11–13]. Here we directly measure the coupled spin–valley dynamics in electron-doped MoS_2 and WS_2 monolayers using optical Kerr spectroscopy, and reveal very long electron spin lifetimes, exceeding 3 ns at 5 K (two to three orders of magnitude longer than typical exciton recombination times). In contrast with conventional III–V or II–VI semiconductors, spin relaxation accelerates rapidly in small transverse magnetic fields. Supported by a model of coupled spin–valley dynamics, these results indicate a novel mechanism of itinerant electron spin dephasing in the rapidly fluctuating internal spin–orbit field in TMDCs, driven by fast inter-valley scattering. Additionally, a long-lived spin coherence is observed at lower energies, commensurate with localized states. These studies provide insight into the physics underpinning spin and valley dynamics of resident electrons in atomically thin TMDCs.

Studies of optical spin orientation and spin relaxation using polarized light have a long and exciting history in conventional III–V and II–VI semiconductors[14,15]. Early seminal works focused on magneto-optical studies of polarized PL from recombining excitons[14], from which spin lifetimes could be indirectly inferred. However, it was the direct observation of very long-lived spin coherence of resident electrons in materials such as GaAs and ZnSe (refs 15,16)—revealed unambiguously by time-resolved Faraday and Kerr rotation studies—that captured widespread interest and helped to launch the burgeoning field of 'semiconductor spintronics' in the late 1990s (ref. 15). With a view towards exploring coupled spin/valley physics of resident electrons in the new atomically thin and direct-bandgap TMDC semiconductors, here we apply related experimental methods and directly reveal surprisingly long-lived and coherent spin dynamics in monolayer MoS_2 and WS_2.

Figure 1a depicts the experimental set-up. High-quality monolayer crystals of n-type MoS_2 and WS_2, grown by chemical vapour deposition on SiO_2/Si substrates[17], were selected on the basis of low-temperature reflectance and PL studies (see Methods). Transverse magnetic fields (B_y) were applied using external coils. A weak pump laser illuminates individual crystals with right- or left-circularly polarized light (RCP or LCP) using wavelengths near the lowest-energy A exciton transition, which primarily photoexcites spin-polarized electrons and holes into the K or K' valley, respectively[1–10]. Any induced spin and valley polarization is then detected by means of the optical Kerr rotation (KR) or Kerr ellipticity (KE) that is imparted to a linearly polarized and wavelength-tunable probe laser that is incident normally and focused on to the crystal. Either continuous-wave (c.w.) or pulsed pump/probe lasers can be used; both types of experiments will be discussed.

The diagrams in Fig. 1a depict the conduction and valence bands in the K and K' valleys in a typical monolayer TMDC, along with the relevant spin/valley optical selection rules and scattering processes. In n-type material, the resident spin-up and spin-down electrons in the conduction band of the K (K') valley have densities $n_\uparrow$ and $n_\downarrow$ ($n'_\uparrow$ and $n'_\downarrow$), which all share a common chemical potential in thermal equilibrium. However, following pulsed photoexcitation and fast (~10 ps) recombination with photogenerated holes[9,10], these resident electron densities may be unequal and out of equilibrium, as depicted. This can arise, for example, from many-body correlations while holes are present[18,19], or from unequal nonradiative recombination rates of holes with the optically forbidden electron states (nonradiative processes account for the vast majority of recombination in TMDCs (ref. 5)). Thus, photoexcitation can impart a net spin polarization ($S_z = n_\uparrow - n_\downarrow + n'_\uparrow - n'_\downarrow$) and/or valley polarization ($N_v = n_\uparrow + n_\downarrow - n'_\uparrow - n'_\downarrow$) onto the resident electrons that may remain even after all holes have recombined. (Analogously, weak steady-state photoexcitation can establish a non-equilibrium steady-state polarization of resident electrons.) The intrinsic relaxation dynamics of this polarization, which proceeds without the perturbing influence of the holes, is the principal focus of these studies.

Crucially, any long-lived polarization of the resident electrons can be directly monitored using Kerr spectroscopy. This stands in marked contrast to polarized PL studies, which explicitly require the participation of (and recombination with) a photo-excited hole. Kerr effects depend only on the difference between a material's RCP and LCP absorption and indices of refraction. According to the selection rules in monolayer MoS_2 and related TMDCs (refs 1,2), RCP light near the lowest-energy A exciton in TMDCs couples to the resident electron density $n_\uparrow$ in the K valley. Similarly, LCP light couples to $n'_\downarrow$ in the K' valley. Perturbations to the densities $n_\uparrow$ and

[1]National High Magnetic Field Laboratory, Los Alamos, New Mexico 87545, USA. [2]Theoretical Division, Los Alamos National Laboratory, Los Alamos, New Mexico 87545, USA. [3]Department of Materials Science and NanoEngineering, Rice University, Houston, Texas 77005, USA. *e-mail: crooker@lanl.gov

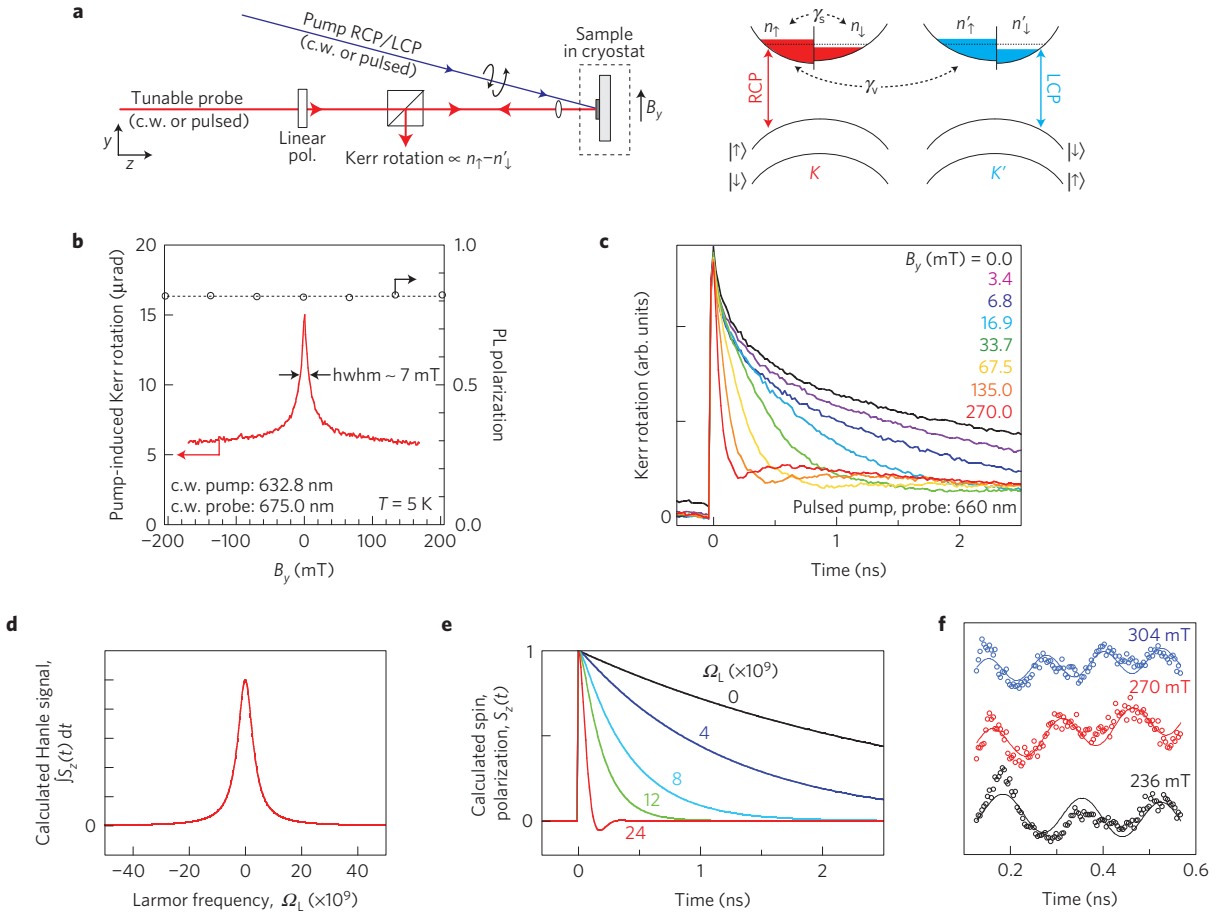

Figure 1 | Long-lived electron spin dynamics in n-type MoS_2 at 5 K. a, Experimental schematic. A weak pump laser illuminates the TMDC crystals with right- or left-circularly polarized (RCP or LCP) light. The induced spin/valley polarization is detected by means of the optical Kerr rotation (KR) or Kerr ellipticity (KE) that is imparted on a linearly polarized, wavelength-tunable probe laser. Pump and probe lasers can be either continuous-wave (c.w.) or pulsed. The diagrams on the right depict a simple single-electron picture of the conduction and valence bands at the K and K' valleys of electron-doped monolayer MoS_2, along with the relevant optical selection rules and scattering processes. In each valley, the conduction bands are separately drawn as spin-up (left) and spin-down (right) components (with slightly different curvature and with small splitting Δ_c; these effects generate the effective spin–orbit field $\pm\hat{z}B_{so}$). The densities of the resident electrons are $n_\uparrow$, $n_\downarrow$, $n'_\uparrow$, and $n'_\downarrow$. Near the lowest-energy A exciton, RCP light couples only to spin-up electron states in the K valley ($n_\uparrow$), whereas LCP light couples only to spin-down electron states in the K' valley ($n'_\downarrow$). Densities $n_\downarrow$ and $n'_\uparrow$ do not couple directly to light at the A exciton energy. Following recombination with photogenerated holes, KR and KE therefore depend on the difference $n_\uparrow - n'_\downarrow$. Electron spin relaxation within a given valley (γ_s) couples $n_\uparrow$ with $n_\downarrow$ (and $n'_\uparrow$ with $n'_\downarrow$), whereas spin-conserving inter-valley scattering γ_v couples $n_\uparrow$ with $n'_\uparrow$ (and $n_\downarrow$ with $n'_\downarrow$). **b**, Using weak c.w. pump and probe lasers, the red curve shows the induced KR versus applied magnetic field B_y from monolayer MoS_2 at 5 K. This Hanle–Kerr experiment reveals rapid reduction of optically induced spin polarization by very small B_y, suggesting long spin relaxation times of resident electrons. The PL polarization (dashed line) shows no change over this field range. **c**, Time-resolved KR data (using pulsed pump and probe lasers) directly reveals very long electron relaxation dynamics in MoS_2, at different B_y. **d**,**e**, Calculated Hanle–Kerr and time-resolved dynamics of itinerant resident electrons, based on the model developed in the main text. Fast inter-valley scattering γ_v and associated fluctuating $\pm\hat{z}B_{so}$ drives the rapid dephasing of electron spin polarization in small B_y. **f**, Expanded view of residual long-lived electron spin coherence, probably due to additional contributions from localized states (curves offset for clarity).

$n'_\downarrow$ shift their chemical potentials, which change the absorption and refraction of RCP and LCP probe light, particularly at wavelengths near optical transitions. Thus, to leading order, Kerr signals using light near the A exciton are proportional to $n_\uparrow - n'_\downarrow$, to which both spin and valley polarization can contribute, namely $(S_z + N_v)/2$.

Figure 1b demonstrates optically induced polarization in monolayer MoS_2 using c.w. pump and probe lasers. The wavelengths λ_{pump} (632.8 nm) and λ_{probe} (675 nm) were chosen to address only the A exciton. At zero applied field, a steady-state KR of ~15 μrad is induced by the pump onto the probe laser. Surprisingly, this polarization signal is sharply reduced by very small transverse fields B_y. The narrow and nearly Lorentzian-shaped dependence of the measured KR on B_y (only ~7 mT half-width) strongly suggests a long-lived spin polarization of resident electrons. (In contrast, the PL polarization, which probes primarily short-lived excitons, is unchanged over this field range, in agreement with earlier studies[7].) These Kerr data are very reminiscent of traditional Hanle-effect studies in conventional semiconductors such as n-type GaAs (refs 14,20,21), wherein B_y dephases an optically injected steady-state electron spin polarization (S_z) owing to spin precession about B_y. This leads to a Lorentzian dependence of S_z on B_y, from which the spin lifetime τ_s can be inferred using the half-width B_{y0} of the Hanle peak if the g-factor g_e is known; namely, $\tau_s^{-1} = g_e \mu_B B_{y0}/\hbar$.

It is therefore tempting to associate the data in Fig. 1b with spin dephasing in MoS_2 due solely to precession of resident electrons about B_y, and to infer a spin lifetime. However, in contrast to conventional III–V or II–VI semiconductors, electrons in the high-momentum K and K' valleys of monolayer MoS_2 are theoretically

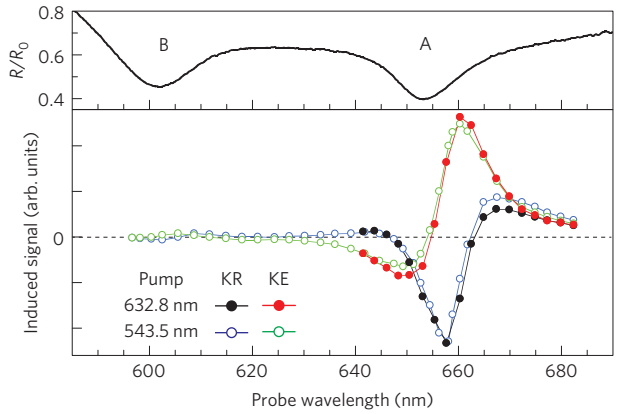

Figure 2 | Spectral dependence of the optically induced Kerr rotation/ellipticity signals in monolayer MoS_2. The upper (black) trace shows the normalized reflectance spectrum R/R_0 from a MoS_2 crystal at 5 K. A and B exciton features are clear. The lower traces show the optically induced KR and KE signals as a function of the probe laser wavelength at $B_y = 0$. A strong resonance at the A exciton is observed. Results using two different pump laser wavelengths are shown (632.8 nm and 543.5 nm; the latter is scaled for ease of comparison).

predicted to experience strong spin–orbit coupling, due to the different curvature of the spin-up and spin-down conduction bands, and also to any additional intrinsic splitting Δ_c of these bands[1,2,22–24]. This coupling can be viewed as a large out-of-plane effective magnetic field $\mathbf{B}_{so}$ (of the order of 10 T, depending on electron density). Importantly, $\mathbf{B}_{so}$ is oriented parallel or antiparallel to $\hat{z}$, depending on whether the electron resides in the K or K' valley. Spin-conserving inter-valley electron scattering, which is not forbidden in the conduction band and which is expected to be fast in these materials ($\gamma_v^{-1} \sim 0.1$–1 ps) given the low electron mobility and the dominant role of impurity scattering, therefore leads to a rapidly fluctuating effective magnetic field 'seen' by electrons.

This fluctuating field alone will not affect (dephase) electron spins that are also oriented along $\pm\hat{z}$. However, in the additional presence of B_y, electron spins will precess about the total fluctuating field $\hat{y}B_y \pm \hat{z}B_{so}$, which is no longer oriented along $\hat{z}$. This leads to a valley-dependent spin precession and associated dephasing that is analogous to the momentum-dependent spin precession and dephasing common in conventional semiconductors (for example, the Dyakonov–Perel mechanism[14]) or to electron spin depolarization in germanium, which is also driven by inter-valley scattering[25]. A direct and testable consequence is that electron spin relaxation in MoS_2 is expected to depend strongly on B_y—even for small B_y—in marked contrast to ordinary III–V and II–VI bulk semiconductors.

The narrow Hanle–Kerr data in Fig. 1b are consistent with this scenario. However, to directly measure electron spin relaxation and test this hypothesis, we turn to time-resolved KR studies using ultrafast lasers. Figure 1c shows the measured decay of the optically induced electron polarization in the same MoS_2 crystal, using photons with energy just below the A exciton resonance. A key finding of this work is that the polarization decay time is extremely long (~3 ns) at zero field. This timescale exceeds typical PL recombination times by two to three orders of magnitude[9,10], further implicating resident electrons as the source of long-lived polarization. Recent studies of monolayer MoS_2 and WSe_2 using related techniques did not reveal any long-lived polarization imparted to resident electrons, perhaps owing to elevated temperatures[13] or to the use of probe photons with higher energy[11,12]. The nanosecond electron spin relaxation observed here at zero field may ultimately be limited by intra-valley Dyakonov–Perel or Elliot–Yafet processes[26,27] (potentially due to long-wavelength flexural phonons[28]), or by spin-flip scattering with magnetic impurities.

Crucially, the polarization decay time decreases rapidly with small increasing B_y, and no prominent spin precession is observed. These two observations directly support the scenario described above, of depolarization due to a rapidly fluctuating $\mathbf{B}_{so}$ driven by fast inter-valley electron scattering, for the following two reasons: first, if $\mathbf{B}_{so}$ were small or did not exist, then pronounced spin precession about B_y would be observed (as is the case for resident electrons in GaAs, ZnSe, GaN, or CdTe (refs 15,16,29,30)). Second, if $\mathbf{B}_{so}$ were static and not fluctuating, then spins would be effectively pinned along $\mathbf{B}_{so}$ and the small B_y ($\ll|\mathbf{B}_{so}|$) would have little influence on the long spin decay. Neither of these phenomena were observed. Rather, these data are consistent with a novel spin relaxation mechanism in monolayer TMDCs that is driven by fast inter-valley scattering (rapidly fluctuating $\mathbf{B}_{so}$), and activated by small B_y.

A model of coupled spin–valley dynamics captures the underlying physics and reproduces essential features of the data. The phenomenological equation of motion for the electron spin polarizations $\mathbf{S}^K$ and $\mathbf{S}^{K'}$ in the two valleys reads:

$$\frac{d\mathbf{S}^\tau}{dt} = \boldsymbol{\Omega}_L \times \mathbf{S}^\tau + \tau\Omega_{so}\hat{z} \times \mathbf{S}^\tau - \gamma_s\mathbf{S}^\tau - \gamma_v(\mathbf{S}^\tau - \mathbf{S}^{-\tau})$$

where $\tau = \tau(t) = \pm 1$ is the index for K and K' valleys respectively (inter-valley scattering events flip τ). The first two terms describe

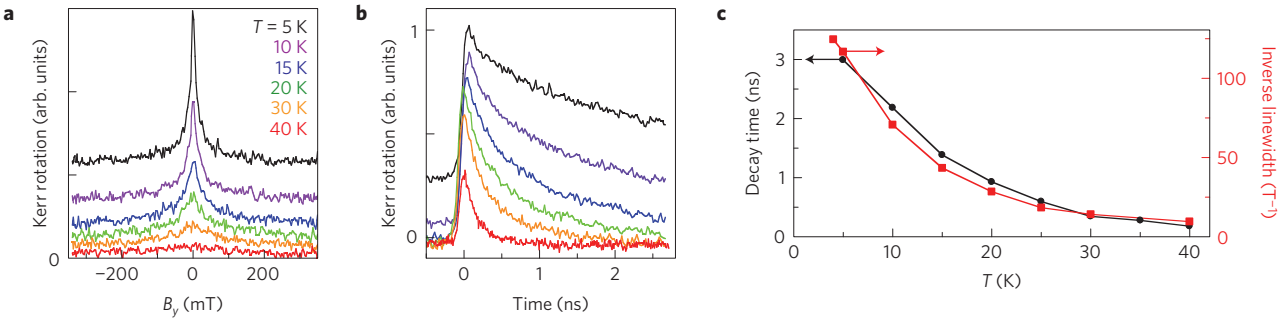

Figure 3 | Temperature dependence of electron spin relaxation in monolayer MoS_2 at zero magnetic field. a, Hanle–Kerr data (using c.w. lasers; $\lambda_{pump} = 632.8$ nm, $\lambda_{probe} = 675$ nm). With increasing temperature, the curve width increases whereas the amplitude drops, indicating faster spin relaxation of resident electrons. **b**, Corresponding time-resolved KR directly reveals faster spin relaxation with increasing temperature. Here, $\lambda_{pump} = 635$ nm with ~100 ps pulse duration; $\lambda_{probe} = 672$ nm with ~250 fs pulse duration. **c**, The measured relaxation time, and inverse Hanle–Kerr linewidth, versus temperature.

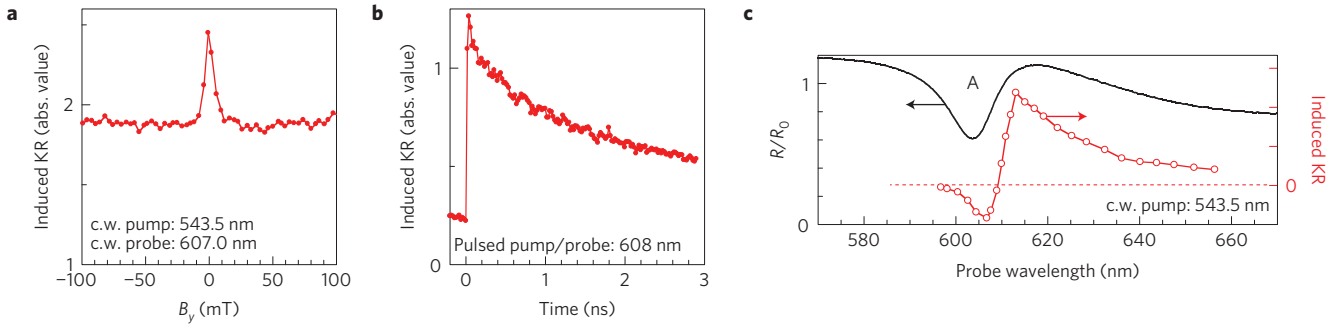

Figure 4 | Long-lived spin polarization dynamics in monolayer WS_2 at 5 K. a, Hanle–Kerr measurement of optically induced spin polarization at the A exciton, using c.w. lasers. (At this probe wavelength the induced KR has a negative sign, thus the absolute value is shown for clarity.) **b**, Time-resolved KR at zero field (using ultrafast pump and probe pulses). **c**, Left axis: normalized reflectivity of monolayer WS_2, showing the A exciton feature. Right axis: wavelength dependence of the optically induced KR signal at zero applied field (using c.w. lasers).

spin precession about an applied field $\mathbf{\Omega}_L = \hat{y} g \mu_B B_y/\hbar$ and the internal spin–orbit field $\mathbf{\Omega}_{so} = \pm\hat{z} g \mu_B B_{so}/\hbar$. The third term describes intrinsic spin relaxation within a given valley with rate γ_s, and the fourth term is spin-conserving inter-valley scattering with rate γ_v, which is expected to be fast and which leads to fast relaxation of any valley polarization. We compute the total spin polarization $\mathbf{S} = \mathbf{S}^K + \mathbf{S}^{K'}$. For large $\mathbf{B}_{so}$ ($\Omega_{so} \gg \Omega_L$) and fast inter-valley scattering ($\gamma_v > \Omega_{so}$), and assuming initial polarization $S_0\hat{z}$, the solution is $S_z(t) = S_0 \sum_{j=1,2} A_j e^{i\omega_j t}$. Here, $A_{1,2} = (1 \pm \Gamma_v/\sqrt{\Gamma_v^2 - \Omega_L^2})/2$ and the two eigenmodes $i\omega_{1,2} = -\gamma_s - \Gamma_v \pm \sqrt{\Gamma_v^2 - \Omega_L^2}$, where $\Gamma_v \equiv \Omega_{so}^2/4\gamma_v$. There is a critical applied field $\Omega_L^c = \Gamma_v$, below which the modes are purely decaying and above which the modes oscillate (see also Supplementary Fig. 4 and accompanying discussion of the complete model). The Hanle curve is calculated by integrating $S_z(t)$ for each Ω_L; namely $\int_0^\infty S_z(t)dt = S_0(\gamma_s + 2\Gamma_v)/[\Omega_L^2 + (\gamma_s^2 + 2\gamma_s\Gamma_v)]$. Thus, Hanle–Kerr data are predicted to be Lorentzian (as observed) with half-width $\sqrt{\gamma_s^2 + 2\gamma_s\Gamma_v}$.

Figure 1d,e shows the calculated Hanle curves and electron spin dynamics. The model reproduces the rapid drop in electron spin polarization with increasing (small) B_y, and captures the shallow dip and subsequent recovery of the electron spin polarization at short timescales. The model does not, of course, capture the offset of the measured Hanle–Kerr data (see Fig. 1b), the origin of which suggests an additional long-lived and field-independent polarization, perhaps from localized states in MoS_2, which have been studied recently. This offset is also manifested in the time-resolved data as the very slowly decaying and largely field-independent signal that persists at long delays.

A surprising additional observation is the appearance, at larger magnetic fields, of a small but long-lived oscillatory signal visible between ~200–800 ps (red trace in Fig. 1c). Figure 1f shows an expanded view of this signal at $B_y = 236$, 270 and 304 mT. The oscillation frequency scales linearly with B_y, indicating that this signal arises from coherently precessing electrons with g-factor $|g_e| \simeq 1.8$. Such long-lived coherence signals are not expected from itinerant resident electrons, for reasons described above. However, they may arise owing to contributions from an additional population of localized states that do not undergo rapid inter-valley scattering and which precess about the bare applied field B_y. Time-resolved measurements at lower photon energies below the A exciton are consistent with this scenario (Supplementary Fig. 1).

We confirm that these Kerr signals originate from MoS_2 by showing their spectral dependence. Figure 2 shows the MoS_2 reflectivity, below which are the peak Hanle–Kerr signals at $B_y = 0$. Both KR and KE show a strong resonance at the A exciton. Data using 632.8 nm and 543.5 nm c.w. pump lasers are shown; the latter allows the induced signals to be tracked out to the higher-energy B exciton, which elicits a smaller response. This behaviour was confirmed on many different MoS_2 crystals. The resonances are redshifted ~25 meV from the exciton peak, suggesting that the resident electrons' polarization may be revealed preferentially through trion-related (rather than neutral exciton-related) optical transitions[2], analogous to studies in III–V and II–VI semiconductor quantum wells[29,30]. The dependence of Hanle–Kerr data on probe wavelength is shown in Supplementary Fig. 2.

An essential consideration for spin-coherent phenomena in semiconductors is its dependence on temperature. Systematic studies on MoS_2 (see Fig. 3) reveal very long spin lifetimes at 5 K (~3 ns), which decrease rapidly to <200 ps by 40 K. This behaviour is in qualitative agreement with recent predictions[28] of Elliot–Yafet spin relaxation processes (within a given valley) due to electron–phonon scattering with long-wavelength flexural phonons. A comparison of supported versus unsupported monolayer crystals could confirm this mechanism.

Finally, we show that these long-lived electron spin polarizations are not unique to MoS_2, but also appear in other TMDCs. Figure 4 shows Hanle–Kerr and time-resolved KR measurements in monolayer WS_2, along with their spectral dependence. WS_2 also exhibits very narrow Hanle–Kerr signals and nanosecond polarization relaxation times. The peak Hanle–Kerr signal also occurs on the low-energy side of the A exciton, again suggesting that coupling to resident electrons may proceed preferentially through trion transitions. The field-independent background on the Hanle data is significantly larger (about 80% of the peak, rather than 30–40% for MoS_2), which may result from lesser material quality or, possibly, the larger spin–orbit splitting in WS_2. Together, these measurements open the door for systematic studies of the detailed interplay between spin–orbit coupling, chemical potential, and spin/valley dynamics of resident carriers in new doped two-dimensional TMDC semiconductors.

Methods

Methods and any associated references are available in the online version of the paper.

Received 25 March 2015; accepted 29 June 2015;
published online 3 August 2015

References

1. Xiao, D., Liu, G.-B., Feng, W., Xu, X. & Yao, W. Coupled spin and valley physics in monolayers of MoS_2 and other group-VI dichalcogenides. *Phys. Rev. Lett.* **108,** 196802 (2012).
2. Xu, X., Yao, W., Xiao, D. & Heinz, T. F. Spin and pseudospins in layered transition metal dichalcogenides. *Nature Phys.* **10,** 343–350 (2014).
3. Mak, K. F., McGill, K. L., Park, J. & McEuen, P. L. The valley Hall effect in MoS_2 transistors. *Science* **344,** 1489–1492 (2014).

4. Splendiani, A. *et al.* Emerging photoluminescence in monolayer MoS_2. *Nano Lett.* **10,** 1271–1275 (2010).
5. Mak, K. F., Lee, C., Hone, J., Shan, J. & Heinz, T. F. Atomically thin MoS_2: A new direct-gap semiconductor. *Phys. Rev. Lett.* **105,** 136805 (2010).
6. Zeng, H., Dai, J., Yao, W., Xiao, D. & Cui, X. Valley polarization in MoS_2 monolayers by optical pumping. *Nature Nanotech.* **7,** 490–493 (2012).
7. Sallen, G. *et al.* Robust optical emission polarization in MoS_2 monolayers through selective valley excitation. *Phys. Rev. B* **86,** 081301(R) (2012).
8. Jones, A. M. *et al.* Optical generation of excitonic valley coherence in monolayer WSe_2. *Nature Nanotech.* **8,** 634–638 (2013).
9. Lagarde, D. *et al.* Carrier and polarization dynamics in monolayer MoS_2. *Phys. Rev. Lett.* **112,** 047401 (2014).
10. Wang, G. *et al.* Valley dynamics probed through charged and neutral exciton emission in monolayer WSe_2. *Phys. Rev. B* **90,** 075413 (2014).
11. Zhu, C. R. *et al.* Exciton valley dynamics probed by Kerr rotation in WSe_2 monolayers. *Phys. Rev. B* **90,** 161302(R) (2014).
12. Plechinger, G., Nagler, P., Schuller, C. & Korn, T. Time-resolved Kerr rotation spectroscopy of valley dynamics in single-layer MoS_2. Preprint at http://arxiv.org/abs/1404.7674 (2014).
13. Dal Conte, S. M. *et al.* Valley and spin dynamics in monolayer MoS_2. Preprint at http://xxx.tau.ac.il/abs/1502.06817 (2015).
14. Meier, F. & Zakharchenya, B. P. (eds) *Optical Orientation: Modern Problems in Condensed Matter Sciences* Vol. 8 (North-Holland, 1984).
15. Awschalom, D. D., Loss, D. & Samarth, N. (eds) in *Semiconductor Spintronics and Quantum Computation* (Nanoscience and Technology Series, Springer, 2002).
16. Kikkawa, J. M., Smorchkova, I. P., Samarth, N. & Awschalom, D. D. Room-temperature spin memory in two-dimensional electron gases. *Science* **277,** 1284–1287 (1997).
17. Najmaei, S. *et al.* Vapor phase growth and grain boundary structure of molybdenum disulfide atomic layers. *Nature Mater.* **12,** 754–759 (2013).
18. Mai, C. *et al.* Many-body effects in valleytronics: Direct measurement of valley lifetimes in single-layer MoS_2. *Nano Lett.* **14,** 202–206 (2014).
19. Singh, A. *et al.* Coherent electronic coupling in atomically thin $MoSe_2$. *Phys. Rev. Lett.* **112,** 216804 (2014).
20. Dzhioev, R. I. *et al.* Low-temperature spin relaxation in n-type GaAs. *Phys. Rev. B* **66,** 245204 (2002).
21. Furis, M. *et al.* Local Hanle-effect studies of spin drift and diffusion in n:GaAs epilayers and spin-transport devices. *New J. Phys.* **9,** 347 (2009).
22. Kormányos, A. *et al.* Monolayer MoS_2: Trigonal warping, the Γ′ valley, and spin–orbit coupling effects. *Phys. Rev. B* **88,** 045416 (2013).
23. Kośmider, K., González, J. W. & Fernández-Rossier, J. Large spin splitting in the conduction band of transition metal dichalcogenide monolayers. *Phys. Rev. B* **88,** 245436 (2013).
24. Tse, W.-K., Saxena, A., Smith, D. L. & Sinitsyn, N. A. Spin and valley noise in two-dimensional Dirac materials. *Phys. Rev. Lett.* **113,** 046602 (2014).
25. Li, P. K., Li, J., Qing, L., Dery, H. & Appelbaum, I. Anisotropy-driven spin relaxation in germanium. *Phys. Rev. Lett.* **111,** 257204 (2013).
26. Ochoa, H. & Roldan, R. Spin-orbit-mediated spin relaxation in monolayer MoS_2. *Phys. Rev. B* **87,** 245421 (2013).
27. Wang, L. & Wu, M. W. Electron spin relaxation due to D'yakonov-Perel' and Elliot-Yafet mechanisms in monolayer MoS_2: Role of intravalley and intervalley processes. *Phys. Rev. B* **89,** 115302 (2014).
28. Song, Y. & Dery, H. Transport theory of monolayer transition-metal dichalcogenides through symmetry. *Phys. Rev. Lett.* **111,** 026601 (2013).
29. Zhukov, E. A. *et al.* Spin coherence of a two-dimensional electron gas induced by resonant excitation of trions and excitons in CdTe/(Cd,Mg)Te quantum wells. *Phys. Rev. B* **76,** 205310 (2007).
30. Chen, Z., Carter, S. G., Bratschitsch, R. & Cundiff, S. T. Optical excitation and control of electron spins in semiconductor quantum wells. *Physica E* **42,** 1803–1819 (2010).

Acknowledgements

We gratefully acknowledge D. L. Smith and H. Dery for helpful discussions, and W. D. Rice for laser expertise. This work was supported by the Los Alamos LDRD programme. These optical studies were performed at the National High Magnetic Field Laboratory, which is supported by NSF DMR-1157490 and the State of Florida. We also acknowledge the support from AFOSR (grant FA9550-14-1-0268) and the Welch Foundation (grant C1716).

Author contributions

L.Y. and S.A.C. conceived and built the experiments. W.C., J.Y., J.Z. and J.L. grew the samples. L.Y. performed the optical measurements. N.A.S. provided theoretical insight. L.Y., N.A.S. and S.A.C. wrote the paper in consultation with all authors.

Additional information

Supplementary information is available in the online version of the paper. Reprints and permissions information is available online at www.nature.com/reprints. Correspondence and requests for materials should be addressed to S.A.C.

Competing financial interests

The authors declare no competing financial interests.

Methods

High-quality triangular crystals of n-type (electron doped) monolayer MoS_2 and WS_2 were grown by chemical vapour deposition on SiO_2/Si substrates, following ref. 17. Typical lateral dimensions ranged from 10–20 μm. The background (residual) electron doping level in these crystals is estimated to be $n_e \sim 5 \times 10^{12}$ cm^{-2} on the basis of transport studies of field-effect transistor devices fabricated from similarly grown single-monolayer crystals. The samples were mounted on the vacuum cold finger of a small variable-temperature liquid helium optical cryostat (3–300 K). Applied magnetic fields up to 300 mT were generated using an external electromagnet. Individual crystals were screened for a high degree of circularly polarized exciton PL (>80%) and sharp reflectivity spectra.

All Kerr-effect measurements were performed in a reflection geometry, as depicted in Fig. 1a. For Hanle–Kerr measurements of steady-state polarization, continuous-wave (c.w.) pump and probe lasers were used. The 632.8 nm and 543.5 nm lines of HeNe lasers were used for the pump, whereas the probe laser was typically a tunable narrowband dye laser or fixed-wavelength diode lasers. Time-resolved measurements used ultrafast 250 fs pulses from a wavelength-tunable 76 MHz optical parametric oscillator (OPO). Time-resolved studies typically used wavelength-degenerate pump and probe pulses (an exception is the temperature-dependent data of Fig. 3, where a 635 nm pulsed diode laser with ∼100 ps pulse duration was synchronized to the OPO and used as a non-degenerate pump laser). In all experiments, the pump laser was weakly focused so as to illuminate the entire TMDC crystal, thereby mitigating any possible influence of density gradients or carrier diffusion, whereas the linearly polarized and normally incident probe laser was more tightly focused to a ∼4 μm spot in the centre of the crystal. It was verified that the small off-axis angle of the pump laser (about 10 degrees from sample normal) did not influence the results—similar data were obtained with co-propagating normally incident pump and probe lasers.

Except where otherwise noted, the pump laser polarization was modulated between RCP and LCP by a photoelastic modulator to facilitate lock-in detection. Detection of the induced optical polarization rotation (KR) and ellipticity (KE) imparted on to the probe beam was achieved with a standard optical bridge arrangement using balanced photodiodes. Low-power pump and probe beams were used, as it was observed that the Hanle widths and polarization decay rates increased with increasing pump and/or probe power. Typical average probe power was in the tens of μW, whereas the pump was in the range from 100–1,000 μW, depending on wavelength and temperature.